sustainability

MDPI

Article

Numerical Analysis and Experimental Study of Unsteady Flow Characteristics in an Ultra-Low Specific Speed Centrifugal Pump

Yangyang Wei [1], Yuhui Shi [1], Weidong Shi [2,*] and Bo Pan [3]

[1] National Research Center of Pumps, Jiangsu University, Zhenjiang 212013, China
[2] School of Mechanical Engineering, Nantong University, Nantong 226019, China
[3] Shandong Xinchuan Mine Electromechanical Equipment Co., Ltd., Jining 272300, China
* Correspondence: wdshi@ntu.edu.cn; Tel.: +86-0511-88799918

Abstract: Low specific speed centrifugal pumps are widely used in urban water supply, agricultural irrigation, petrochemical and other fields due to their small flow rate and high head. Therefore, the study of unsteady flow characteristics plays a vital role in its safe and stable operation. In this paper, numerical simulation and experimental methods are used to explore the unsteady performance of the pump. The results show that the fluctuations of the external characteristic such as head, shaft power and energy loss are due to the periodic disturbance of the flow field of pump. But the transient performance of shaft power and head shows different changing trends due to different influencing factors. In this paper, the transient process of hydraulic performance is divided into three stages according to the causes and characteristics of hydraulic fluctuations. Most of the hydraulic losses occur inside the impeller, so the impeller flow field determines the level of time average hydraulic performance. Although the hydraulic loss of the spiral case is small, it is greatly affected by the rotor-stator interaction, which affects the strength of the hydraulic fluctuation. This study is of great significance to the mechanism of rotor-stator interaction and the stable operation of low specific speed centrifugal pumps.

Keywords: low specific speed; transient pulsation; hydraulic performance; rotor-stator interaction

Citation: Wei, Y.; Shi, Y.; Shi, W.; Pan, B. Numerical Analysis and Experimental Study of Unsteady Flow Characteristics in an Ultra-Low Specific Speed Centrifugal Pump. *Sustainability* **2022**, *14*, 16909. https://doi.org/10.3390/su142416909

Academic Editor: Domenico Mazzeo

Received: 27 October 2022
Accepted: 9 December 2022
Published: 16 December 2022

1. Introduction

From the perspective of energy saving, ultra-low specific speed centrifugal pumps are widely used in various fields of social development, and their safe and efficient operation has attracted much attention [1,2]. Their specific speed is not greater than 30, and these pumps has the characteristics of small flow and high head. Due to the relatively small geometric size of the ultra-low specific speed centrifugal pump, its internal flow is complex when pumping viscous fluid, often accompanied by turbulent flow such as cavitation, secondary flow, axial eddy current, and complex pressure pulsation signals [3,4]. This also results in a low hydraulic efficiency. At present, the research on ultra-low specific speed centrifugal pump mainly focuses on two aspects: design optimization and internal flow characteristics research [5–7].

Zhao et al. [8] adopted a genetic algorithm based on NSGA-II to optimize the design of a centrifugal pump with a specific speed of 30. Based on the Plackett-Burman test, the parameters were screened to obtain the optimal geometric parameters of the impeller of the centrifugal pump. After optimization, the hydraulic efficiency was increased by about 5.82%. The quadratic regression orthogonal composite method was used to optimize low specific speed centrifugal pumps in the study of Zhong et al. [9]. They took 7 main geometric parameters of the impeller as research factors and discovered that the blade number played a dominant role in improving the hydraulic performance of the centrifugal pump. Zhang et al. [10] optimized the design of the impeller blade wrap angle of an

ultra-low specific speed centrifugal pump based on the Bezier curve. It was found that the centrifugal pump efficiency reached a maximum when the blade wrap angle was 120°. Sato et al. [11] and Daqiqshirazi et al. [12] optimized the shape of the pump casing in order to reduce the disc friction loss of the ultra-low specific speed centrifugal pump.

Scholars have also done a lot of research on the influence of different pump structures on the pump performance. Siddique et al. [13,14] studied the influence of splitter blades on the hydraulic performance of an ultra-low specific speed centrifugal pump, and the results showed that splitter blades can reduce the amplitude of pressure pulsation as well as hydraulic loss, and improve the hydraulic performance of the pump. Gao et al. [15] studied the influence of blade trailing edge profile on the performance and unsteady pressure fluctuation of a centrifugal pump. It was found that, when the pressure surface of the blade was elliptical or both sides of the blade were elliptical, the pump efficiency was significantly improved, and the pressure fluctuation was also reduced. Chabannes et al. [16] analyzed the effect of volute throat area on the performance of ultra-low specific speed centrifugal pumps. Within a certain range, the pump head and efficiency increased by increasing the throat area.

The external characteristics of centrifugal pumps are the external manifestations of internal flow features, such as rotational stall and rotor-stator interaction, which often lead to the hump and unsteady fluctuations of the external characteristic curve. Based on numerical simulation, Zeng et al. [17] and Cui et al. [18] studied the fluid excitation phenomenon in an ultra-low specific speed centrifugal pump and its influence on the dynamic characteristics of the rotor. The results indicated that the main frequency of the pressure pulsation was the passing frequency of the impeller blades, and the pressure pulsation amplitude of the main frequency was much larger than that of the secondary main frequency. Zhang et al. [19] conducted research on the unsteady flow field of an ultra-low specific speed centrifugal pump by PIV test. At low flow rate, there was a typical jet wake flow pattern at the blade outlet. However, this pattern was not obvious at large flow rate because the high-momentum fluid was concentrated on the suction side of the blade. Ye et al. [20–22] conducted a research on the ultra-low specific speed centrifugal pump and discovered that the liquid flow angle at the inlet of the pump impeller channel was relatively larger due to the strong separation flow and the evolution of the vortex. Besides, many researchers had studied the internal flow of ultra-low specific speed centrifugal pumps through experiments and numerical simulations, such as the pressure pulsation, radial force, and vortex dynamics [23–26].

According to the above discussion, there are relatively few studies on the internal velocity fluctuation, the velocity-pressure coupling characteristics under the influence of rotor-stator interaction, and its effects on the internal flow field. In order to study this problem, this paper mainly discusses the influence mechanism of rotor-stator interference on the pump energy characteristics and the unsteady variation of the pressure on the impeller-volute interface. And Through numerical simulation and experimental analysis, it is proposed that the SST k-w turbulence model is more suitable for ultra-low specific speed centrifugal pumps. In addition, the research in this paper also enriches the coupling mechanism of the velocity field and the pressure field in the ultra-low specific speed centrifugal pump, and provides a theoretical basis and reference for its stable operation.

2. Numerical Methods

2.1. Centrifugal Pump Parameters

The basic external characteristic parameters of the centrifugal pump include head and efficiency. The dimensionless head coefficient ϕ and efficiency η are defined as:

$$\phi = \frac{gH}{0.5u_2^2} \tag{1}$$

$$\eta = \frac{(P_2 - P_1)Q}{W_s} \tag{2}$$

where H is the head, m; u_2 is the circumferential velocity at the impeller outlet, m/s; P_1 and P_2 are the inlet and outlet total pressures, Pa; W_s is the shaft power, W; Q is the flow rate, m^3/s; g is the acceleration due to the gravity, m/s^2.

To qualitatively analyze the change in the internal pressure of the pump, it is necessary to analyze the time-averaged value and pulsation pattern of pressure. The time-averaged value of the pressure pulsation is defined as:

$$\overline{p} = \frac{1}{N}\sum_{i=1}^{N} p(i) \tag{3}$$

The equation for the coefficient of RMS pressure fluctuations (root mean square) can be expressed as follows:

$$C_{Psdv} = \frac{\sqrt{\frac{1}{N}\sum_{i=1}^{N}(p(i)-\overline{p})^2}}{0.5\rho u_2^2} \tag{4}$$

where $p(i)$ is the instantaneous pressure of the measuring point, Pa; $\overline{p}$ is the average pressure, Pa. When the number of samples is high enough, the root mean square change of the pressure fluctuation coefficient is very small, which equals to a constant. And the dimensionless pressure fluctuation amplitude is defined as follows:

$$C_P = \frac{p(i)-\overline{p}}{0.5\rho u_2^2} \tag{5}$$

where ρ is the medium density, kg/m^3.

2.2. Total Pressure Loss Coefficient

The internal flow field of the centrifugal pump can be considered as periodic flow. The total pressure loss of flow passage components, namely hydraulic loss, can be calculated by using the total pressure difference. The total pressure drop coefficient of the volute is defined as follows:

$$\phi_s = \frac{P_{w,in,tp} - P_{w,out,tp}}{0.5\rho {u_2}^2} \tag{6}$$

The total pressure rise coefficient of impeller is defined as follows:

$$\phi_r = \frac{P_{r,out,tp} - P_{r,in,tp}}{0.5\rho {u_2}^2} \tag{7}$$

where *out* is the outlet of the component; *in* is the inlet of component; *tp* represents the total pressure, Pa; The subscripts w and r represent the volute and impeller, respectively.

The dimensionless coefficient of impeller work is defined as follows:

$$W_{sft} = \frac{2\pi Mn}{60 u_2 A_2 0.5\rho u_2^2} \tag{8}$$

where A_2 is the outlet area of the impeller.

3. Numerical Model and Setting

3.1. Experimental System

Figure 1 shows the test rig of the model pump. The motor and pump are fixed on the metal mounting plate, and several pressure monitoring points are arranged at the circumferential position of the volute to measure the internal pressure pulsation. The sensor parameters are given in Table 1. The accuracy of the instrument refers to the percentage of its allowable error in the dial scale value.

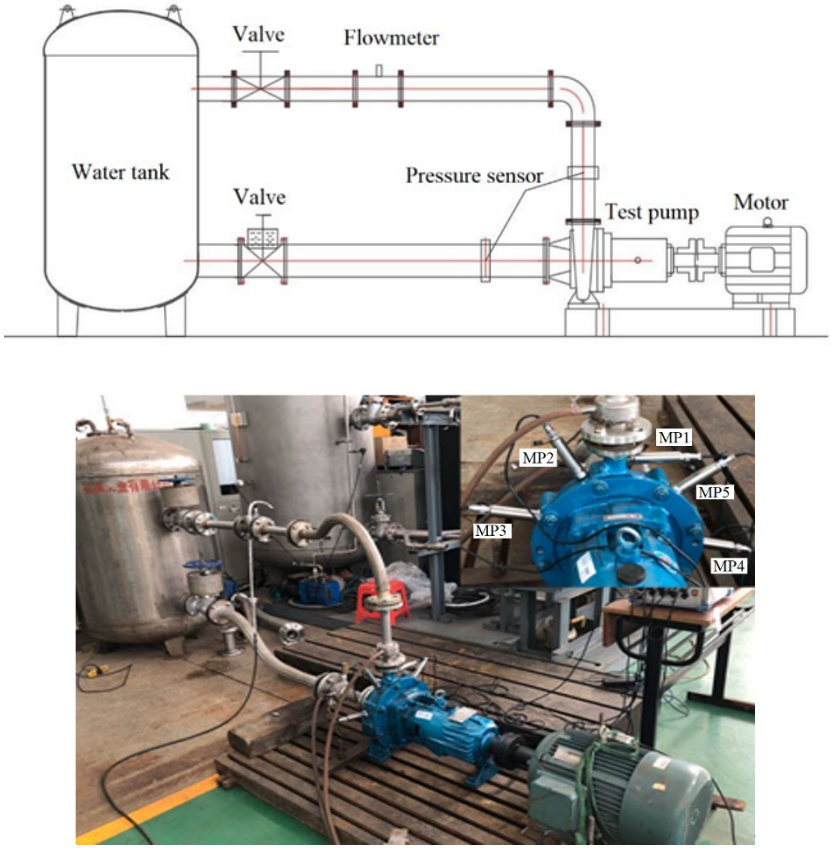

Figure 1. The test rig of the centrifugal pump.

Table 1. Parameters of the sensor.

Sensor	Model	Range	Precision
Flowmeter	LW-40	0~25 m^3/h	±0.5%
Inlet pressure sensor	WT2000	−0.1~0.1 MPa	±0.1%
Outlet pressure sensor	WT2000	0~1.6 MPa	±0.1%
High-frequency dynamic pressure sensor	CY200	0~2.0 MPa	±0.1%
Temperature sensor	PT100	0~100 °C	±0.5%

3.2. Model Parameter Settings

The key parameters of the model pump used in this study are shown in Table 2. The specific speed ns is defined as the following equation:

$$n_s = \frac{3.65 \times n_d \times \sqrt{Q_{des}}}{H_{des}^{0.75}} \tag{9}$$

where the units of all variables are consistent with those in Table 2. The mesh for numerical simulations is generated by the ANSYS ICEM. The computational domains of the pump mainly include the inlet pipe, the impeller, the volute, and the outlet pipe. In order to obtain a relatively stable flow field, the length of the inlet and outlet pipes is set to be 10 times the pipe diameter. Hexahedral mesh is used in the computational domain and mesh refinement is performed on key parts such as blade surface and volute tongue. In order to ensure the accuracy of data transmission and capture the flow characteristics at the interface of different computational domains, mesh refinement is performed at the interface of different computational domains. The mesh division is shown in Figure 2.

Table 2. Parameters of the pump model.

Parameter	Value
Rotating speed n_d (r/min)	2900
Design flow rate Q_{des} (m^3/h)	10
Design head H_{des} (m)	80
Pump inlet diameter D_1 (mm)	50
Pump outlet diameter D_2 (mm)	20
Outlet width of impeller (mm)	6.5
Exit angle of blade (°)	25
Volute tongue inner diameter d_3 (mm)	290
Outlet diameter of impeller D_i (mm)	259
Blade thickness at trailing edge	6
Number of blades Z	3

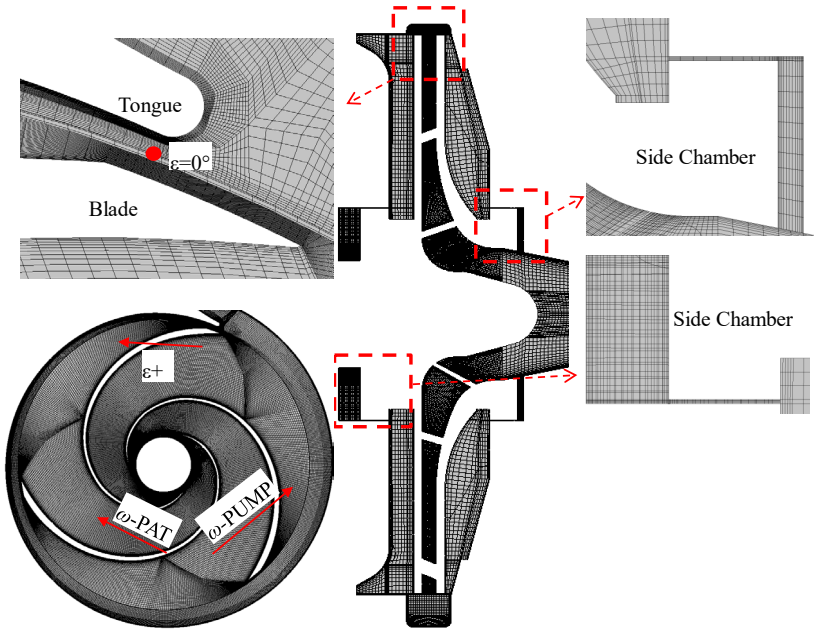

Figure 2. Grid of computational domain.

Figure 3 shows the comparison between the calculated and experimental values at the design condition for different turbulence models [27]. The calculation results of the SST k-ω turbulence model agrees well with the experimental data compared to other turbulent models [28–30]. Thus, it is chosen for the turbulence model of the numerical simulation in this study. The boundary conditions are set as the total pressure at the inlet of the pump, the mass flow at the outlet of the pump. The outlet pressure is set to 1 atm. No-slip wall is applied to all the walls. The interface between the rotor and the stator selects the frozen rotor condition when in the steady calculation and selects the transient rotor-stator condition when in the unsteady calculation [31]. The initial field of transient simulation is set to the result of the steady calculation. The unsteady calculation time step is 5.75×10^{-5} which equals to 1° rotation of the impeller. A transient simulation is conducted for 6 revolutions of the impeller. And the calculation data of the last revolution is chosen for the analysis of the pressure and power fluctuation.

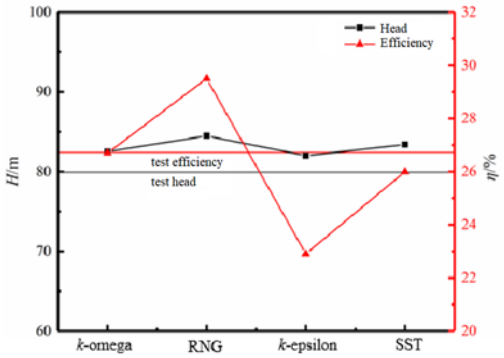

Figure 3. Comparison of external characteristics under different turbulence models.

3.3. Grid Independence Verification

The validation of grid independence is made to ensure the accuracy of simulation results. Three different grids are used to calculate it numerically, and the differences between the experimental and numerical simulation results are compared. The number of cells corresponding to each grid scheme is shown in Table 3.

Table 3. Mesh schemes.

Scheme	Mesh Number
G1	2.01×10^6
G2	5.12×10^6
G3	7.48×10^6

The comparison of the performance between the numerical calculation and experiment is shown in Figure 4a. The head of the pump decreases with the increase of the flow rate. As the number of grids increases, the difference between the experimental head and the numerical head becomes smaller. Considering the computational cost, scheme G2 was selected for numerical simulation in this study. Figure 4b presents the pressure amplitude at the dominant frequency of the monitoring points in Figure 1. The dominant frequency of pressure pulsation obtained by numerical simulation and experiment both occurs at the blade frequency, and the amplitude is similar.

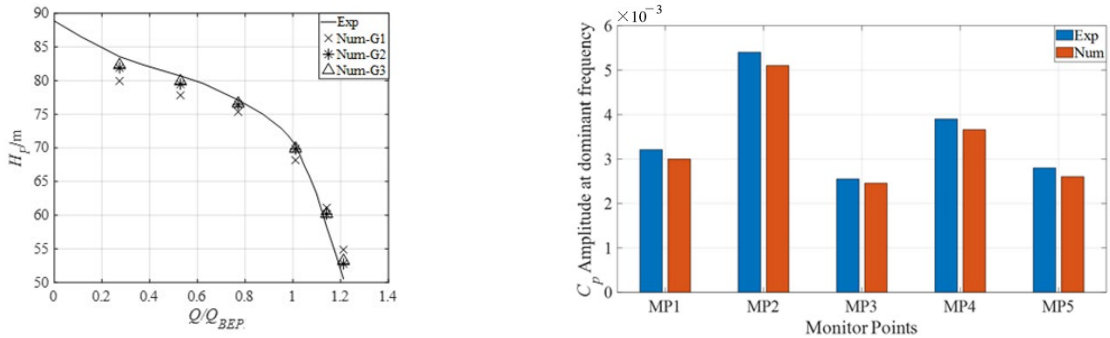

(**a**) External performance (**b**) Pressure amplitude at the dominant frequency

Figure 4. Validation of grid independence.

4. Results and Discussions

Figure 5 shows the unsteady head of the pump in one rotation cycle. Here, ε is the angle between the trailing edge of the blade and the volute tongue. The ε is zero when the blade trailing edge is passing the tongue. The head gradually increases with the decrease in flow rate. The head coefficient shows obvious periodic fluctuation, and the fluctuation

law is similar under different discharge. It is well understood that the number of cycles is the same as the number of blades of the impeller. Therefore, the key to the problem is the reason that affects the transient change trend. For the minimum value of pulsation, it is obviously the interaction between the fluid at the tail of the impeller and the tongue. In particular, there is a quadratic fluctuation at the valley of the curve shown in Figure 5. This may be related to the rotor-stator interaction between the impeller and the tongue. When the pressure side of the blade sweeps across the tongue, its unsteady head reaches the minimum value. With the rotation of the blade, a secondary fluctuation occurs when the suction side of the blade sweeps across the tongue. As the blade continues to rotate, the unsteady head gradually rises to the maximum value. Therefore, the blade thickness may be the cause of secondary fluctuation. The comprehensive fluctuation of the unsteady head coefficient is closely related to the unsteady flow field.

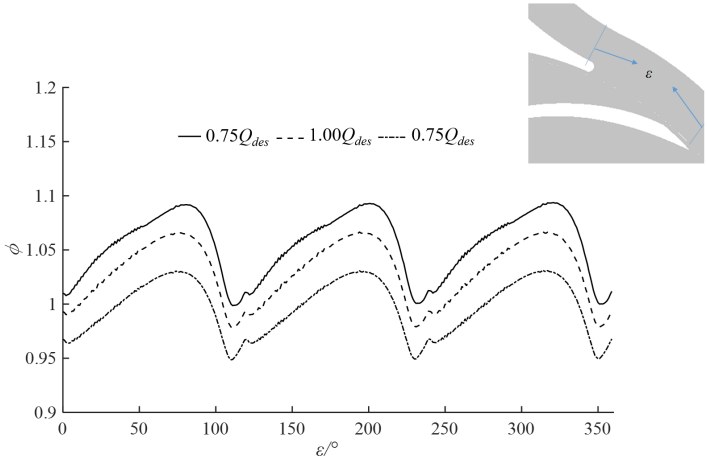

Figure 5. Transient change of head coefficient for three flow rates.

Figure 6 shows the unsteady fluctuation curve of the impeller shaft power during one impeller rotation. The shaft power increases with the increase of the flow rate, and the oscillation trend of the shaft power coefficient curve is similar under different flow rates, which shows obvious periodic fluctuations. With the blades rotating from the tongue, the shaft power rapidly increases to a maximum value. The reduction of shaft power will go through three stages. First, the shaft power will slowly decrease, then increase in a gentler trend, and finally, rapidly reduce to the minimum value. Compared with Figure 5, when the blade rotates 120°, there is no secondary fluctuation like the head coefficient, which indicates that the influence of this transient effect on the impeller is very weak.

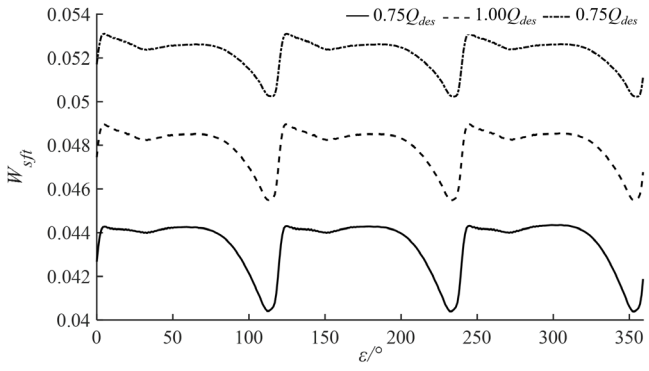

Figure 6. Transient change of shaft power coefficient for three flow rates.

Within one cycle of the impeller, the pressure rises of impeller and pressure drop of volute are shown in Figure 7. With the increase in the flow rate, the pressure rise coefficient

in the impeller presents a decreasing trend while it has the opposite trend in the volute. Moreover, the pressure rise coefficient of the impeller is close to the head coefficient, which means that most of the water losses occur in the impeller. Therefore, the flow field in the impeller determines the hydraulic performance. However, the fluctuation of the impeller pressure rise coefficient is 0.01 times of the head coefficient and mainly occurs near the tongue, which indicates that the loss of the impeller is not the main reason for determining the hydraulic fluctuation. The pressure drop coefficient of volute is very small, but the fluctuation is more obvious, and the fluctuation amplitude can be close to 0.1. Therefore, although the hydraulic loss of volute is small, it is the main factor affecting the fluctuation range of hydraulic performance. This also indirectly shows that the rotor-stator interaction has a greater impact on the flow field of the volute.

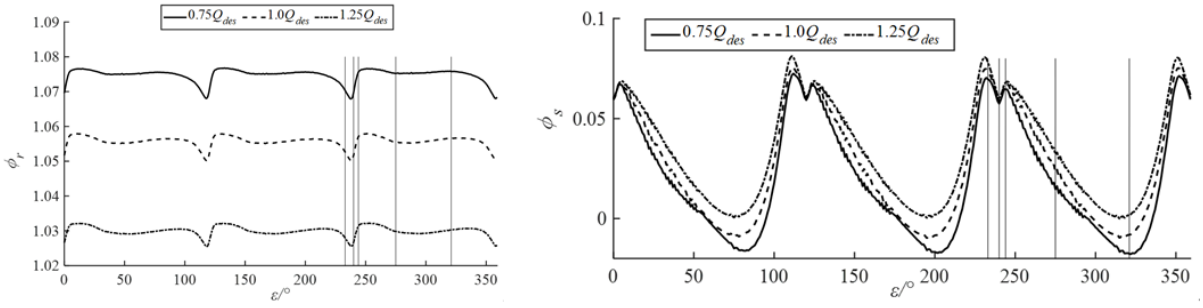

(**a**) Impeller (**b**) Volute

Figure 7. Transient change of pressure coefficient at three flow rates.

Before studying the large hydraulic fluctuation of the volute, it is necessary to explore the hydraulic loss and flow characteristics of the impeller. Figure 8 shows the average value and variance distribution of pressure in the mid-span section of the pump. The time-averaged values of turbulent kinetic energy and dissipation rate under design flow rate are presented at Figure 9. The pressure increases gradually from the impeller inlet to the outlet. Due to the pressure loss caused by the leakage of the balance hole in the pump casings, the pressure at the impeller inlet is very small. In general, the maximum pressure appears in the impeller outlet. With the increasing flow rate, pressure of inlet gradually increases. As can be seen from the oval marked area, the low pressure is mainly distributed in the region around the impeller inlet. The maximal variance value of the pressure occurs on the interface of the impeller and volute, especially in the regions near the blade trailing edge. As the flow rate increases, the pressure at the inlet of the impeller also increases, causing the head to drop. As shown in Figure 9, the dissipation of turbulent kinetic energy mainly occurs at the balance hole at the impeller inlet. This is the main reason for inducing hydraulic loss. Since it is far from the interface between impeller and volute and located in the upstream area, it is less subject to rotor-stator interaction. Therefore, the pressure rise coefficient of the impeller changes slightly, and only changes greatly before and after passing through the tongue.

One cycle of the above four external characteristic curves is shown in Figure 10a, and five typical blade rotation angles are shown in Figure 10b. The positions are named T1, T2, T3, T4, and T5 in chronological order. The three flow channels are named C1, C2 and C3 in anticlockwise direction. For convenience, the interface between impeller and volute is hereinafter referred to as interface. Figure 10a more clearly proves that the hydraulic performance can be affected by changing the hydraulic loss and flow field characteristics of the impeller under different flow rates. However, the hydraulic fluctuation characteristics under different flow rates are similar, which is mainly controlled by the flow field in the volute. The rotor-stator interaction mainly affects the flow field of the volute, and the mechanism of this influence will be explained later. There are very similar fluctuation characteristics under different flows, however, the following article pays more attention to

the transient changes of hydraulic characteristics in a cycle. Therefore, only the flow field characteristics of design flow are studied to obtain the mechanism of rotor-stator interaction on hydraulic performance.

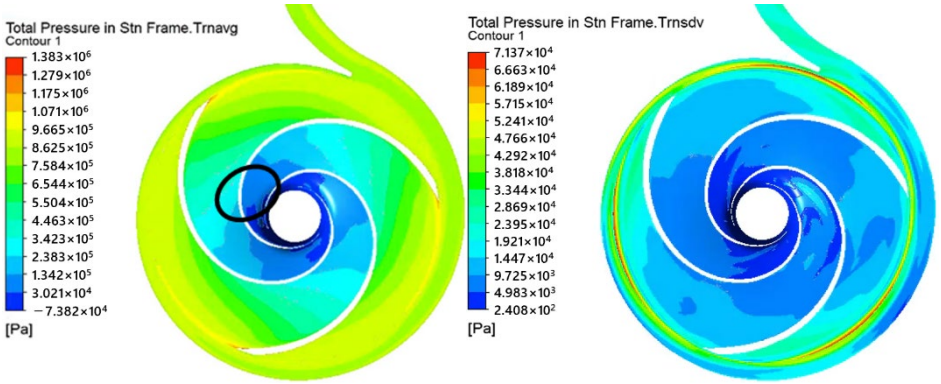

(**a**) $0.75Q_{des}$

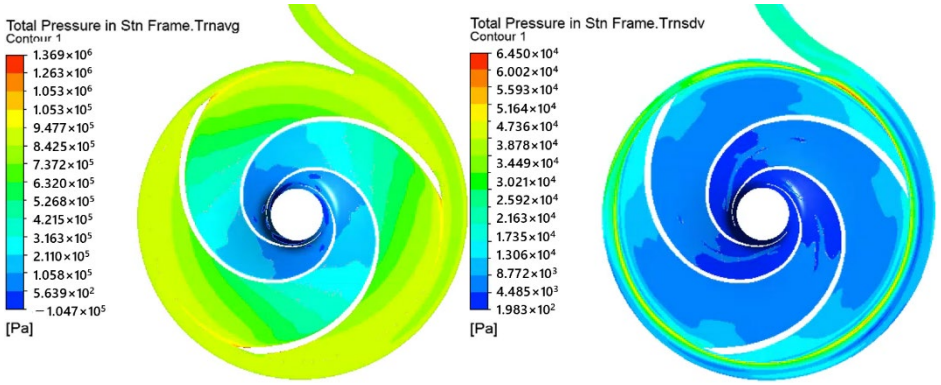

(**b**) $1.0Q_{des}$

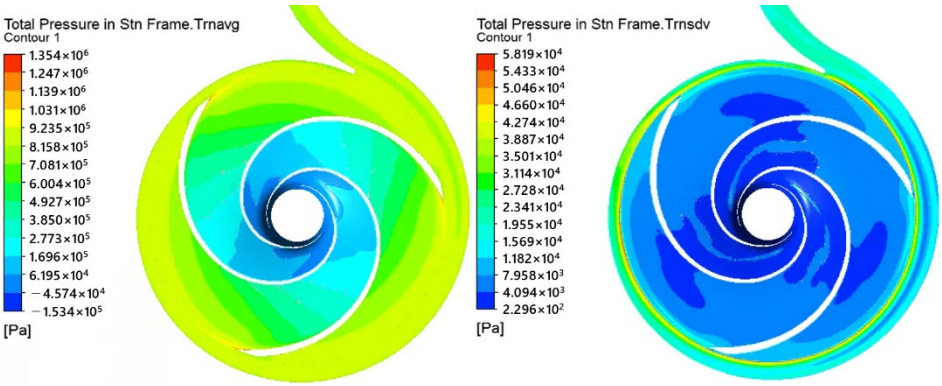

(**c**) $1.25Q_{des}$

Figure 8. Mean value and variance distribution of total pressure at mid-span surface under three flow rates.

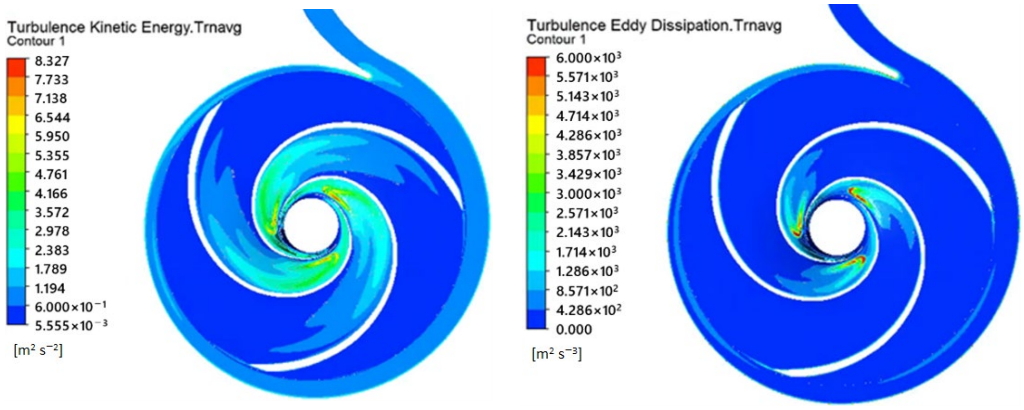

Figure 9. Mean distribution of turbulent kinetic energy and turbulent eddy dissipation rate at Q_{des}.

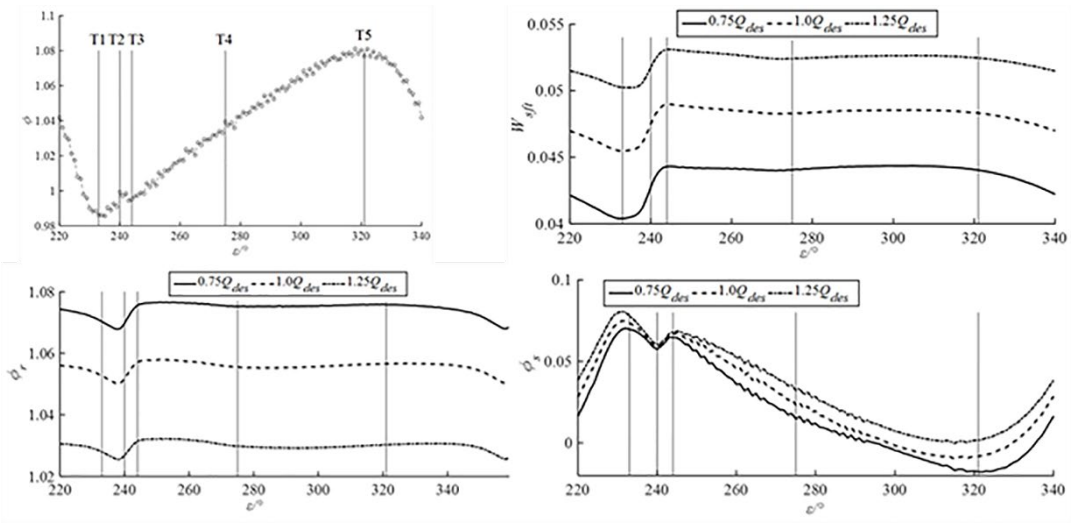

(**a**) Performance change in 1/3 impeller rotation cycle

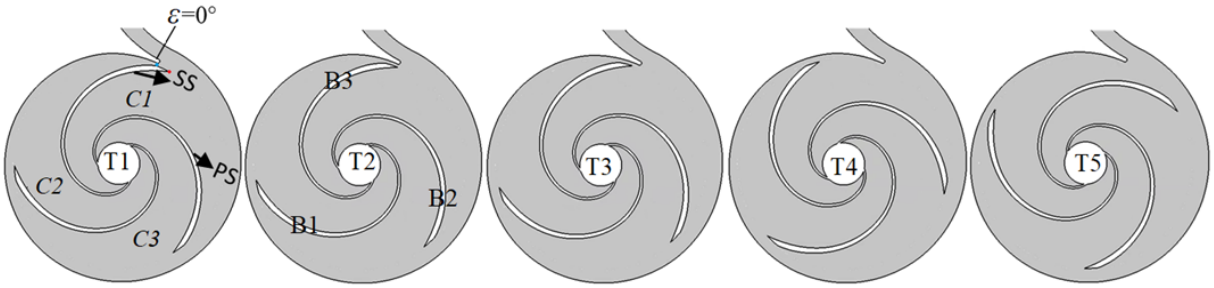

(**b**) position of impeller corresponding to typical time

Figure 10. Performance change characteristics of 1/3 impeller in rotating cycle.

According to Figure 10a, the hydraulic performance change process can be divided into three stages according to the shaft power. In the first stage (T1~T3): the power rise period, the shaft power increases, and the head first increases and then decreases. In the second stage: power stability period (T3~T5), shaft power is stable and head increases. In the third stage (T5~T1): power reduction period, shaft power and head decrease. The hydraulic loss of the volute basically presents the opposite trend to the head. The analysis of the transient characteristics of the flow field at the interface is of great significance to the study of the rotor-stator interaction of centrifugal pumps. Figure 11 shows the distribution of radial velocity and circumferential velocity at the interface, in which HS represents the hub surface and SS represents the shroud surface. And the contours from top to button

corresponds to the position of T1, T2, T3, T4, T5 in turn. The velocity distribution at the inlet will directly affect the flow field and energy loss in the volute. The radial velocity difference at different times is small, but the inflow at time T5 is better than that at time T1. This indicates that the volute has lower energy loss and the head will increase at T5. The high value of circumferential velocity is distributed in the region of y/b = 0.25~0.75. The width of the volute inlet is twice that of the impeller outlet, so the area where y/b = 0.0~0.25 is the front pump casing, and the area where y/b = 0.75~1 is the rear pump casing. The area near the vanes and pump casing has a slightly slower speed. Similar to the radial velocity, the flow field from T1 to T3 has no obvious change, but the flow field at T4 and T5 has been significantly improved, which will also improve the hydraulic performance. In addition, for the flow passage near the tongue, the radial velocity and circumferential velocity have large gradients, which makes the fluid have a certain impact on the impeller. Therefore, the impeller shaft power will also change between T1 and T3 (the blade goes across the tongue).

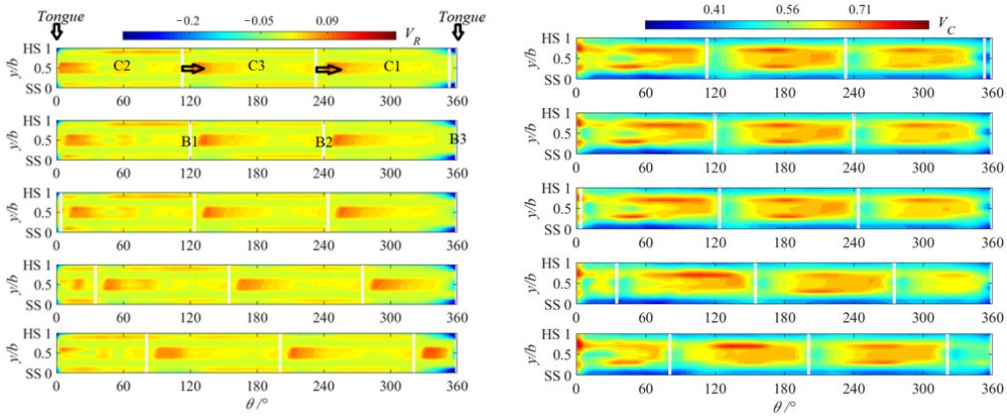

(**a**) Radial velocity (**b**) Circumferential velocity

Figure 11. Velocity Field at Interface.

Internal pressure distribution of pump determines the variation of fluid mechanical energy and the transmission of shaft power. Figure 12 shows velocity vector and pressure distribution at interface. Obviously, the pressure fluctuation gradient at T2 is smaller than T1 and T3. This resulted in a small fluctuation of loss coefficient and head at T2. T4 and T5 are similar to the velocity field, and the inlet pressure field of the volute has been further improved. High pressure area and low-pressure area are produced on the left and right sides of the tongue, which affect the flow field near the tongue. To further study the flow field characteristics that cause this phenomenon, the pressure and velocity vectors at the mid-span position in the 180° area near the tongue are selected to obtain Figure 12b. The red dotted line represents the tongue, and the red solid line represents the suction side of the trailing edge of the blade. They are respectively the blue point and the red point in Figure 10b. The solid black line represents the pressure. At time T3, the blade has started to move away from the tongue. With the increase of time, the flow field on the left side of the tongue has been improved. The distance between the tongue and the right blade is not enough to cause greater interaction. Therefore, at T5, the hydraulic loss of the volute is the smallest and the head coefficient is the largest. However, after T5, as the blade approaches the tongue, the tail jet will cause great impact near the tongue, which leads to rapid increase of hydraulic loss and reduction of head. The velocity vector distribution of T1, T2 and T3 has little difference. However, according to the conclusion in Figure 12a and the relative position of the blade and tongue, it can be inferred that the small fluctuations at T2 are related to the thickness of the blade. Assuming that the blade has no thickness, the changes of various hydraulic properties will be monotonic during T1–T5. However, due to the

thickness and tangential trailing edge structure of the blade, the flow field near the trailing edge is distorted greatly, so a small secondary wave is finally generated.

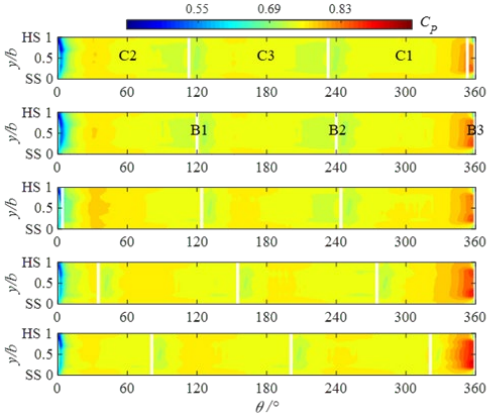

(**a**) Pressure distribution of interface

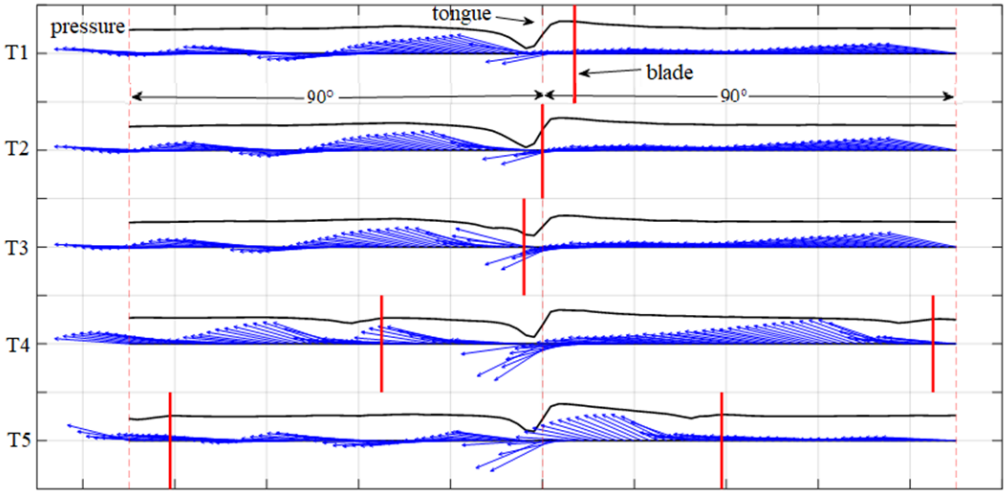

(**b**) Velocity vector and pressure at mid-span position

Figure 12. Velocity vector and pressure distribution at interface.

5. Conclusions

To study the transient fluctuation characteristics of ultra-low specific speed centrifugal pump, numerical simulation and experimental methods were applied. The unsteady flow pattern is studied by analyzing the hydraulic performance and pressure loss coefficient under different flow rates. According to the characteristics of the internal flow field, the mechanism of the rotor-stator interaction that causes the transient changes is discussed.

(1) The head of the numerical simulation presents a good agreement with that of the experimental data. And the maximum error of hydraulic head is calculated to be lower than 5% at the selected grid scheme. Thus, the numerical results in this study are fairly reliable.

(2) The number of cycles of all hydraulic characteristics is equal to the number of blades, and the hydraulic performance shows a similar change trend under different flow rates. But the transient performance of shaft power and head shows different changing trends due to different influencing factors. Most of the hydraulic losses occur inside the impeller, so it is the impeller flow field that determines the level of time averaged hydraulic performance. The hydraulic loss of volute is small, but it determines the fluctuation range of hydraulic performance.

(3) The hydraulic loss and turbulent dissipation in the impeller mainly occur near the balance hole, so it is less affected by rotor-stator interaction, about 10% of the total fluctuation range. The circumferential velocity and pressure distribution at the volute inlet show obvious changes with time. The effect of rotor-stator interaction on the flow field in the volute is more significant.

(4) According to the characteristics and causes, the transient hydraulic performance is divided into three stages. In the period of power increase, the rotor-stator interaction is the strongest, causing the increase of shaft power. However, due to the thickness of the blade and the structural form of the trailing edge, the loss in volute and head of pump have non-linear changes. During the power stability period, the rotor-stator interaction has little influence on the impeller, and the continuously improved flow field improves the hydraulic performance. During the power reduction period, the distance between the blade and the tongue is shortened, which makes the blade wake flow have a greater impact on the tongue, resulting in increased hydraulic loss.

Author Contributions: Conceptualization, Y.W. and W.S.; methodology, Y.W. software, Y.S.; validation, W.S. and B.P.; formal analysis, Y.S.; investigation, Y.W.; resources, W.S.; data curation, Y.S.; writing—original draft preparation, Y.W.; visualization, W.S. and B.P.; supervision, Y.W. and Y.S.; project administration, W.S. All authors have read and agreed to the published version of the manuscript.

Funding: This work was supported by the Jiangsu Province Universities Natural Sciences Foundation (Grant No. 20KJB570002), Project of self-made experimental instruments and equipment of Jiangsu University (Grant No. ZZYQSB202206), National Natural Science Foundation of China (Grant No. 51979138), and National key research and development program (Grant No. 2019YFB2005300).

Institutional Review Board Statement: Not applicable.

Informed Consent Statement: Not applicable.

Data Availability Statement: Not applicable.

Conflicts of Interest: The authors declare no conflict of interest.

Nomenclature

A_2	Area of the impeller outlet [m^2]
C_{Psdv}	Coefficient of RMS pressure fluctuation [-]
C_p	Pressure coefficient [-]
D_1	Pump inlet diameter [mm]
D_2	Pump outlet diameter [mm]
D_i	Outlet diameter of impeller [mm]
H_{des}	Design head [m]
f_b	Blade passing frequency [Hz]
g	Acceleration due to the gravity [m/s^2]
k_{AVE}	Time-average of turbulent kinetic energy [m^2/s^2]
ke_{AVE}	Time-average of turbulent eddy dissipation [m^2/s^3]
k_{STD}	Standard deviation of turbulent kinetic energy [-]
ke_{STD}	Standard deviation of turbulent eddy dissipation [-]
M_n	Torque [N·m]
M_P	Torque of the fluid acting on the pressure side of the flow channel [N·m]
M_S	Torque of the fluid acting on the suction side of the flow channel [N·m]
n_d	Rotating speed [r/min]
n_s	Specific speed [-]
N	Number of samples [-]
P_1	Total pressure at the pump inlet [Pa]
P_2	Total pressure at the pump outlet [Pa]
$p(i)$	Pressure at the monitor point [Pa]

$\overline{p}$	Average pressure [Pa]
$P_{w,out,tp}$	Total pressure at the volute outlet [Pa]
$P_{w,in,tp}$	Total pressure at the volute inlet [Pa]
$P_{r,out,tp}$	Total pressure at the impeller outlet [Pa]
$P_{r,in,tp}$	Total pressure at the impeller inlet [Pa]
Q	Flow rate [m^3/s]
Q_{des}	Flow rate at design point [m^3/s]
u_2	Circumferential velocity [m/s]
W_s	Shaft power [W]
W_{sft}	Dimensionless coefficient of impeller work [-]
Z	Number of impeller blades [-]
ϕ	Dimensionless head coefficient [-]
ϕ_S	Total pressure loss coefficient of the volute [-]
ϕ_r	Total pressure loss coefficient of the impeller [-]
η	Efficiency [%]
ρ	Density [kg/m^3]

References

1. Wang, C.; Zhang, Y.; Hou, H.; Yuan, Z.; Liu, M. Optimization Design of an Ultra-Low Specific-Speed Centrifugal Pump Using Entropy Production Minimization and Taguchi Method. *Int. J. Fluid Mach. Syst.* **2020**, *13*, 55–67. [CrossRef]
2. Jia, X.; Cui, B.; Zhu, Z.; Yu, X. Numerical Investigation of Pressure Distribution in a Low Specific Speed Centrifugal Pump. *J. Therm. Sci.* **2018**, *27*, 9. [CrossRef]
3. Wang, C.; Zhang, Y.; Zhu, J.; Yuan, Z.; Lu, B. Effect of cavitation and free-gas entrainment on the hydraulic performance of a centrifugal pump. *Proc. Inst. Mech. Eng. Part A J. Power Energy* **2020**, *235*, 095765092093934. [CrossRef]
4. Wei, Y.; Yang, Y.; Zhou, L.; Jiang, L.; Shi, W.; Huang, G. Influence of Impeller Gap Drainage Width on the Performance of Low Specific Speed Centrifugal Pump. *J. Mar. Sci. Eng.* **2021**, *9*, 106. [CrossRef]
5. Zhang, N.; Gao, B.; Li, Z.; Jiang, Q. Cavitating flow-induced unsteady pressure pulsations in a low specific speed centrifugal pump. *R. Soc. Open Sci.* **2018**, *5*, 180408. [CrossRef]
6. Alemi, H.; Nourbakhsh, S.A.; Raisee, M.; Najafi, A.F. Effect of the volute tongue profile on the performance of a low specific speed centrifugal pump. *Proc. Inst. Mech. Eng. Part A J. Power Energy* **2015**, *229*, 210–220. [CrossRef]
7. Del Rio, A.; Casartelli, E.; Mangani, L.; Roos, D. Assessment of advanced RANS turbulence models for the stability analysis of low specific speed pump-turbines. *IOP Conf. Ser. Earth Environ. Sci.* **2021**, *774*, 205–218. [CrossRef]
8. Zhou, L.; Hang, J.; Bai, L.; Krzemianowski, Z.; El-Emam, M.A.; Yasser, E.; Agarwal, R. Application of entropy production theory for energy losses and other investigation in pumps and turbines: A review. *Appl. Energy* **2022**, *318*, 119211. [CrossRef]
9. Zhong, W.; Zhou, J.; Zhou, S. The Effects of Different Splitter Blades Number on Characteristics of Miniature Super-Low Specific Speed Centrifugal Pump. *IOP Conf. Ser. Earth Environ. Sci.* **2021**, *772*, 012065. [CrossRef]
10. Zhang, R.H.; Guo, R.; Yang, J.H.; Luo, J.Q. Inverse Method of Centrifugal Pump Impeller Based on Proper Orthogonal Decomposition (POD) Method. *Chin. J. Mech. Eng.* **2017**, *30*, 1025–1031. [CrossRef]
11. Sato, K.; Shigemitsu, T. Research on Performance Improvement of Low Specific Speed Centrifugal Pump. *Proc. Mech. Eng. Congr. Jpn.* **2017**, *2017*, J0550101. [CrossRef]
12. DaqiqShirazi, M.; Torabi, R.; Riasi, A.; Nourbakhsh, S.A. The effect of wear ring clearance on flow field in the impeller sidewall gap and efficiency of a low specific speed centrifugal pump. *Arch. Proc. Inst. Mech. Eng. Part C J. Mech. Eng. Sci. 1989–1996* **2017**, *232*, 095440621772942. [CrossRef]
13. Siddique, M.H.; Samad, A.; Hossain, S. Centrifugal pump performance enhancement: Effect of splitter blade and optimization. *Proc. Inst. Mech. Eng. Part A J. Power Energy* **2022**, *236*, 391–402. [CrossRef]
14. Chabannes, L.; Tefan, D.; Rudolf, P. Effect of Splitter Blades on Performances of a Very Low Specific Speed Pump. *Energies* **2021**, *14*, 3785. [CrossRef]
15. Gao, B.; Zhang, N.; Li, Z.; Ni, D.; Yang, M. Influence of the Blade Trailing Edge Profile on the Performance and Unsteady Pressure Pulsations in a Low Specific Speed Centrifugal Pump. *J. Fluids Eng. Trans. ASME* **2019**, *138*, 051106. [CrossRef]
16. Chabannes, L.; Tefan, D.; Rudolf, P. Volute throat area and wall modelling influence on the numerical performances of a very low specific speed pump. *IOP Conf. Ser. Earth Environ. Sci.* **2021**, *774*, 012007. [CrossRef]
17. Zeng, G.; Li, Q.; Wu, P.; Qian, B.; Huang, B.; Li, S.; Wu, D. Investigation of the impact of splitter blades on a low specific speed pump for fluid-induced vibration. *J. Mech. Sci. Technol.* **2020**, *34*, 2883–2893. [CrossRef]
18. Cui, B.; Zhang, Y.; Huang, Y.; Zhu, Z. Analysis of unsteady flow and fluid exciting forces of multistage centrifugal pump based on actual size. *Proc. Inst. Mech. Eng. Part A J. Power Energy* **2022**, *236*, 21–32. [CrossRef]
19. Zhang, N.; Gao, B.; Li, Z.; Ni, D.; Jiang, Q. Unsteady flow structure and its evolution in a low specific speed centrifugal pump measured by PIV. *Exp. Therm. Fluid Sci.* **2018**, *97*, 133–144. [CrossRef]

20. Ye, W.; Luo, X.; Huang, R.; Jiang, Z.; Li, X.; Zhu, Z. Investigation of flow instability characteristics in a low specific speed centrifugal pump using a modified partially averaged Navier–Stokes model. *Proc. Inst. Mech. Eng. Part A J. Power Energy* **2019**, *233*, 834–848. [CrossRef]
21. Gu, Y.; Li, J.; Wang, P.; Cheng, L.; Qiu, Y.; Wang, C.; Si, Q. An Improved One-Dimensional Flow Model for Side Chambers of Centrifugal Pumps Considering the Blade Slip Factor. *J. Fluids Eng.* **2022**, *144*, 091207. [CrossRef]
22. Gu, Y.; Cheng, J.; Wang, P.; Cheng, L.; Si, Q.; Wang, C.; Shouqi, Y. A Flow Model for Side Chambers of Centrifugal Pumps Considering Radial Wall Shear Stress. *Proc. Inst. Mech. Eng. Part C J. Mech. Eng. Sci.* **2022**, *236*, 09544062211073023. [CrossRef]
23. Lu, G.; Zuo, Z.; Sun, Y.; Liu, D.; Tsujimoto, Y.; Liu, S. Experimental evidence of cavitation influences on the positive slope on the pump performance curve of a low specific speed model pump-turbine. *Renew. Energy* **2017**, *113*, 1539–1550. [CrossRef]
24. El-Emam, M.; Zhou, L.; Yasser, E.; Bai, L.; Shi, W. Computational methods of erosion wear in centrifugal pump: A state-of-the-art review. *Arch. Comput. Methods Eng.* **2022**, *29*, 3789–3814. [CrossRef]
25. Yang, Y.; Zhou, L.; Zhou, H.; Lv, W.; Wang, J.; Shi, W.; He, Z. Optimal Design of Slit Impeller for Low Specific Speed Centrifugal Pump Based on Orthogonal Test. *J. Mar. Sci. Eng.* **2021**, *9*, 121. [CrossRef]
26. Zhang, N.; Jiang, J.; Gao, B.; Liu, X.; Ni, D. Numerical analysis of the vortical structure and its unsteady evolution of a centrifugal pump. *Renew. Energy* **2020**, *155*, 748–760. [CrossRef]
27. Han, Y.; Zhou, L.; Bai, L.; Shi, W.; Agarwal, R. Comparison and validation of various turbulence models for U-bend flow with a magnetic resonance velocimetry experiment. *Phys. Fluids* **2021**, *33*, 125117. [CrossRef]
28. Al-Obaidi, A.R. Effects of different turbulence models on three-dimensional unsteady cavitating flows in the centrifugal pump and performance prediction. *Int. J. Nonlinear Sci. Numer. Simul.* **2019**, *20*, 487–509. [CrossRef]
29. Zhang, J.; Li, G.; Mao, J.; Yuan, S.; Qu, Y.; Jia, J. Numerical investigation of the effects of splitter blade deflection on the pressure pulsation in a low specific speed centrifugal pump. *Proc. Inst. Mech. Eng. Part A J. Power Energy* **2020**, *234*, 420–432. [CrossRef]
30. Gu, Y.; Yuan, S.; Pei, J.; Zhang, J.; Zhang, F.; Huang, X. Effects of the impeller–volute tongue interaction on the internal flow in a low-specific-speed centrifugal pump with splitter blades. *Proc. Inst. Mech. Eng. Part A J. Power Energy* **2018**, *232*, 170–180. [CrossRef]
31. Zhang, Y.; Zang, W.; Zheng, J.; Cappietti, L.; Zhang, J.; Zheng, Y.; Fernandez-Rodriguez, E. The influence of waves propagating with the current on the wake of a tidal stream turbine. *Appl. Energy* **2021**, *290*, 116729. [CrossRef]